biomolecules

MDPI

Article

In vitro and in vivo evaluation of ^{99m}Tc-polymyxin B for specific targeting of Gram- bacteria

Sveva Auletta[1], Filippo Galli[1], Michela Varani[1], Giuseppe Campagna[1], Martina Conserva[1], Daniela Martinelli[2], Iolanda Santino[2], Alberto Signore[1*]

[1] Nuclear Medicine Unit, Department of Medical-Surgical Sciences and of Translational Medicine, "Sapienza" University of Rome, Italy; sveva.auletta@hotmail.it; filippo.galli@hotmail.com; varanimichela@gmail.com; gius.campagna@gmail.com; martina.conserva977@gmail.com

[2] Microbiology Unit, Department of Clinical and Molecular Medicine, "Sapienza" University of Rome, Italy; dany.stefano@tiscali.it; iolanda.santino@uniroma1.it

* Correspondence: alberto.signore@uniroma1.it; Tel.: +39-6-33775037

Abstract: BACKGROUND: Infectious diseases are one of the main causes of morbidity and mortality worldwide. Nuclear molecular imaging would be of great help to non-invasively discriminate between septic and sterile inflammation through available radiopharmaceuticals, despite none is currently available for clinical practice. Here, we describe the radiolabelling procedure and *in vitro* and *in vivo* studies of ^{99m}Tc-polymyxin B sulphate (PMB) as a new single photon emission computed tomography (SPECT) imaging agent for the characterization of infections due to Gram-negative bacteria. RESULTS: Labelling efficiency was 97±2% with an average molar activity of 29.5±0.6 MBq/nmole. Product was highly stable in saline and serum up to 6 h. *In vitro* binding assay showed significant displaceable binding to Gram-negative bacteria but not to Gram-positive controls. In mice, ^{99m}Tc-HYNIC-PMB was mainly uptaken by liver and kidneys. Targeting studies confirmed the specificity of ^{99m}Tc-HYNIC-PMB obtained *in vitro*, showing significantly higher T/B ratios for Gram-negative bacteria than Gram-positive controls. CONCLUSIONS: *In vitro* and *in vivo* results suggest that ^{99m}Tc-HYNIC-PMB has a potential for in vivo identification of Gram-negative bacteria in patients with infections of unknown aetiology. However, further investigations are needed to deeply understand the mechanism of action and behaviour of ^{99m}Tc-HYNIC-PMB in other animal models and in man.

Keywords: polymyxin B, infection imaging, bacteria, ^{99m}Tc-polymyxin B

Citation: Auletta, S.; Galli, F.; Varani, M.; Campagna, G.; Conserva, M.; Martinelli, D.; Santino, I.; Signore, A. In vitro and in vivo evaluation of ^{99m}Tc-polymyxin B for specific targeting of Gram- bacteria. *Biomolecules* **2021**, *11*, x. https://doi.org/10.3390/xxxxx

Received: date
Accepted: date
Published: date

1. Introduction

Discrimination between sterile inflammation and infection has always been one of the major challenges for scientific community and for nuclear medicine too. Several radiopharmaceuticals, such as antimicrobial peptides, antibiotics, sugars or antifungal, poorly allows to differentiate between infection and sterile inflammation and also to unmask sites of occult infection. Despite excellent pre-clinical results, none of these radiopharmaceuticals has been introduced into clinics yet, due to poor specificity in man [1-5].

As a matter of facts, radiolabelled leukocyte imaging, with either ^{99m}Tc-HMPAO or ^{111}In-oxine is the scintigraphic imaging test of choice for most infections in the immunocompetent population [6,7].

In some case, such as in spondylodiscitis, the use of [^{18}F] FDG has proved to be more sensitive and specific than radiolabelled white blood cells [8].

Nevertheless, when infection is diagnosed, the problem remains about the identification of the causative agent and haemocultures or needle aspiration (or biopsy) are often necessary to isolate the pathogen. However, ultrasound guided or CT-guided biopsies or

fluid aspiration can result in higher specificity but always with low sensitivity, ranging from 69% to 80% [9-13].

A major improvement for therapy would be to identify, by a simple imaging modality, if the infection is caused by Gram negative (Gram-) or Gram positive (Gram+) bacteria or if it is a fungal infection. In the last 5 years we aimed at synthetizing a new radiopharmaceutical for the specific identification in vivo, by gamma camera imaging, of Gram- infections.

Among the many antimicrobial peptides, we concentrated on polymyxins [14-16]. Polymyxins (A, B, C, D, E or colistin) are decapeptides with molecular weights in the range of 1200 Da, that differ only for few amino acid residues [17]. This class of antimicrobial peptides is characterized from a specific structure consisting of a cyclic heptapeptide ring bound, through a tripeptide side chain, to a hydrophobic fatty acid tail (Figure 1). Despite five polymyxins were described, only polymyxin B and colistin were used for clinical purpose [18].

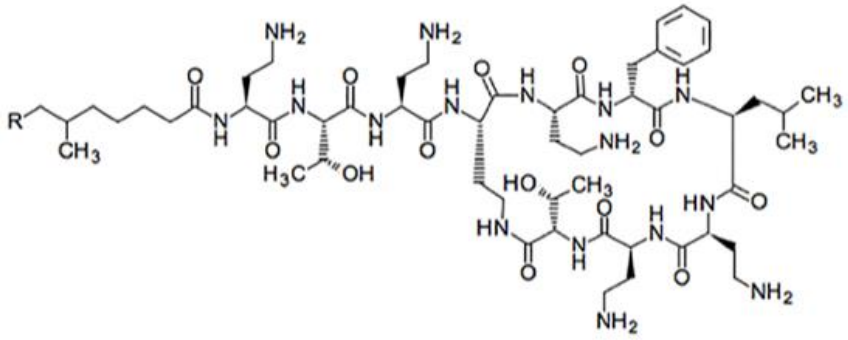

Figure 1. Structural formula of native PMB with a molecular weight of approx. 1200 g/mole.

Studies conducted on the relation between structure-activity of polymyxin B (PMB), demonstrate that PMB acts on lipopolysaccharide (LPS) like an amphipathic antimicrobial peptide: the polar face of the peptide interacts with the polar lipid A component of LPS, while the lipophilic face permeates into the hydrophobic layer of the outer membrane, resulting in disruption of the membrane and in a major susceptibility to other hydrophobic antibiotics [19,20].

Commercially, polymyxin B is available as polymyxin B sulphate, a mixture of polymyxin B_1 and B_2 as prevalent forms and polymyxins $B_{3\text{-}6}$, that differ only for the fatty acid tail [21]. In the last decades, the use of polymyxin B and colistin was renewed due to increase of multidrug-resistant (MDR) Gram- bacterial infections [22] such as due to *Pseudomonas aeruginosa* and *Acinetobacter baumanii,* that are resistant to many available antibiotics [23,24]. Because of the considerable potential of this antimicrobial peptide, in this paper we describe the radiolabelling of polymyxin B sulphate with 99m-Technetium (^{99m}Tc) with the aim to produce a new radiopharmaceutical, with high specific activity, for imaging of Gram- infections. This would allow to inject nanomolar quantities of radiolabelled peptide thus avoiding any side effect.

2. Materials and Methods

2.1. Conjugation

Labelling of polymyxin B sulphate (Sigma Aldrich, St. Louis, MO) was performed with indirect method: PMB molecules were conjugated with a heterobifunctional cross-linker, succinimidyl-6-hydrazinonicotinate hydrochloride (HYNIC), purchased from ABX (advanced biochemical compounds, Radeberg, Germany). HYNIC is able to react with free ε-amino groups of lysine in proteins and to chelate ^{99m}Tc [25].

HYNIC was dissolved in dimethylformamide (70 μM) (DMF; Sigma-Aldrich, St. Louis, MO) and PMB was dissolved in water. They were incubated for 2 h in the dark, at room temperature, using different HYNIC: protein molar ratio. In order to eliminate free SH-NH molecules, the reaction mixture was purified by PD MidiTrap G-10 (GE Healthcare, Waukesha, WI) using distilled water as eluent. The amount of PMB in each fraction was initially determined by bicinchoninic acid (BCA) assay: 25 μL of purified samples were added to 200 μL of BCA reagents in a microplate and incubated at 37 °C for 30 minutes. Subsequently, absorbance at 562 nm was measured with a microplate spectrophotometer (Thermo Fisher Scientific Inc, Waltham, MA) and compared with protein solutions of known concentration.
In other experiments the amount of PMB in fractions was measured by reverse phase HPLC chromatography by standardizing an automatic method for precise quantification of eluted protein on the basis of absorbance at 210 nm, as described below. When compared, BCA assay and HPLC gave identical results. The conjugated product was also analysed by mass spectrometry (MALDI-TOF).

2.2. Radiolabelling procedure

10 μg of conjugated PMB was labelled with 222 MBq of freshly eluted $^{99m}TcO_4$ (100 μL NaCl 0.9%). The reaction was conducted in presence of different amount of co-ligand tricine and reducing agent stannous chloride ($SnCl_2$), in order to obtain the best labelling conditions. Therefore, tricine (Sigma-Aldrich, St. Louis, MO) was dissolved in distilled water and $SnCl_2$ (Sigma-Aldrich, St. Louis, MO) in purged HCl 0.1 M (10 mg/mL).
The reaction solution was incubated for 10 minutes at room temperature and the labelling efficiency (LE) and colloid percentages were evaluated by quality controls.

2.3. Quality controls

LE and colloids percentage were evaluated by instant thin layer chromatography (ITLC) and high-performance liquid chromatography (HPLC).
For iTLC, silica gel strips (Pall LifeSciences, Port Washington, NY) were used as stationary phase, NaCl 0.9% solution as mobile phase for determination of free pertechnetate (Rf=0.9) and NH_3:H_2O:EtOH (1:5:3) solution as mobile phase for colloids (Rf=0.1) determination. iTLC strips were analysed by a radio-scanner (Bioscan, Inc, Poway, CA) and each species was determined.
HPLC was performed with a Gilson system, using a reverse phase chromatography C-18 column (5 mm, 5 μm, 250 x 4.6 mm, Phenomenex, Torrance, CA) and a H_2O (A)/Acetonitrile (B) (Baker, Sanford, ME) gradient (0-5 min 5% B; 5-15 min 5-95% B; 15-18 min 95% B; 18-21 min 95-5% B) with a flow rate of 1 mL/min.
Stability assay was performed adding 100 μL of ^{99m}Tc-HYNIC-PMB to 900 μL of freshly prepared human blood serum or NaCl 0.9%. The vials were incubated at 37 °C and the radiochemical purity was measured at 1, 3, 6, and 24 h by HPLC.

2.4. Micro-organisms

The laboratory strains *Escherichia coli* (ATCC 25922), *P. aeruginosa* (ATCC 27853), *Staphilococcus aureus* (ATCC 25923), *Enterococcus faecalis* (ATCC 29212), *A. baumanii* (ATCC 19606) and *Klebsiella pneumoniae* (ATCC 13883) were used. Bacteria were stored at -70 °C using a cryovial bead preservation system. Single cryovial beads were cultured overnight on Brain Heart Infusion Agar (BHI) for 24 h and, secondly, cultured on blood agar plates to evaluate the replication rate. For *in vitro* studies, a known concentration of bacteria was incubated until reaching the desired concentration of 1×10^8 CFU.

2.5. In vitro binding studies

Binding of ^{99m}Tc-HYNIC-PMB to all bacterial strains were tested *in vitro*. ^{99m}Tc-HYNIC-PMB was diluted 1:100 in NaCl 0.9%, and 250 μL transferred to vials pre-filled with 500 μL of bacteria (10^8 CFU) and with a correct volume of NaCl 0.9%+1% of bovine

serum albumin (BSA) to reach a final volume of 1 mL. Vials with bacterial cells were incubated at 37 °C and 4 °C to study whether the temperature influences the binding. Binding assay was also performed in the presence and in the absence of 100-fold excess of unlabelled PMB in order to investigate the displacement of the radiopharmaceutical. The binding to bacteria was calculated at different time points (10 min, 30 min and 1 h), by centrifugation of vials for 10 minutes at 20000 g at 4 °C. Pellets were washed with 1 mL of NaCl 0.9%+1% of BSA and centrifuged again for 10 minutes at 20000 g. Pellets were then re-suspended in 1 mL of NaCl 0.9%+1% of BSA. Supernatants and re-suspended pellets were counted in a single-well NaI γ-counter (AtomLab, 500-Biodex) and the counts per minute (CPM) recorded. The percentage of ^{99m}Tc-HYNIC-PMB in the pellets was calculated as CPM/CPM_0, where CPM were associated to pellets and CPM_0 the CPM of pellet plus CPM of supernatant.

2.6. Biodistribution studies

All applicable institutional and/or national guidelines for the care and use of animals were followed.

The physiological distribution of ^{99m}Tc-HYNIC-PMB was determined in healthy C57BL/6 mice (female, 6-10 weeks old, Envigo): 1.85 MBq (50 μL, 0.1 mg) of radiolabelled PMB was injected in the lateral tail vein of mice. Images were acquired under anaesthesia using a high resolution γ-camera (Li-Tech, Italy) at 1, 3, and 6 h.

After each time point, four mice were sacrificed; blood samples and major organs (small bowel, large bowel, kidneys, spleen, stomach, liver, muscle, bone, lungs and salivary glands) were collected and weighted for ex-vivo studies. The radioactivity in each vial was counted in a single-well gamma counter (PerkinElmer, Waltham, MA).

Radioactivity in all organs was expressed as percentage of injected dose per organ (%ID) and percentage of injected dose per gram (%ID/g).

2.7. Targeting studies

The specificity of ^{99m}Tc-HYNIC-PMB to localize infectious foci was investigated in C57/BL6 mice (female, 6-10 weeks old, Envigo). The infection was inducted by the injection of 3 different amounts of bacteria (10^7, 10^8 and 10^9 CFU for *E. coli*, *P. aeruginosa*, *A. baumanii*, *S. aureus* and *E. faecalis*) in right thigh in 100 μL of extracellular matrix (ECM)-based hydrogel (Matrigel®, Corning). This compound allows to obtain a focused and high concentration infection in the mouse thigh. As control, mice received an injection of ECM-based hydrogel alone in the contralateral thigh with the aim to induce a sterile inflammatory reaction, as previously demonstrated [26]. For each dose of bacteria, 4 mice were used in order to have reproducible and statistically significant data. Imaging was performed 24 h after the injection of bacteria at 1, 3 and 6 h after the injection of ^{99m}Tc-HYNIC-PMB in the lateral tail vein (1.85 MBq, 50 μL, 0.1 μg). Planar images were acquired using high resolution planar γ-camera (Li-Tech, Italy), under anaesthesia. Each animal was acquired for the same imaging time, adjusting the scan time to dose. After imaging session at 6 h, mice were sacrificed. From each infected thigh, we removed the infected area that resulted inflamed at visual inspection. From contralateral thigh, we removed an equivalent volume of tissue where ECM-based hydrogel was administered. All removed tissues were weighted and counted using a single-well gamma counter (PerkinElmer, Waltham, MA). A few mice were also studied up to 24 h p.i. but best time points for all experiments were set at 3 and 6 h p.i. due to rapid binding of PMB to bacteria.

The radioactivity was expressed as percentage of injected dose per organ (%ID) and percentage of injected dose per gram (%ID/g). For each time point, the in vivo target-to-background ratios (T/B ratios) were measured by calculating the activity in two regions of interest (ROI) of same size, over the infected thigh (target) and contralateral non-infected thigh (background).

2.8. Statistical analysis

Statistical analysis was performed using SAS v. 9.4 (SAS, Institute Inc., Cary, NC, USA). All results were showed as mean ± SD. Shapiro-Wilk test was used to verify the normality of distribution of continuous variables. Comparisons of *in vitro* binding results were analysed by t Student test (HOT vs. 100x cold). Multiple comparisons were performed by Benjamini-Hochberg (FDR). A probability level of $p<0.05$ was considered to be statistically significant.

3. Results

3.1. Radiolabelling

The highest labelling efficiency (LE) was obtained using HYNIC:PMB ratio of 1.5:1, tricine:$SnCl_2$ ratio of 50:1, obtaining a LE of 97±2% and an amount of colloids <10% as showed in Figure 2 and 3.

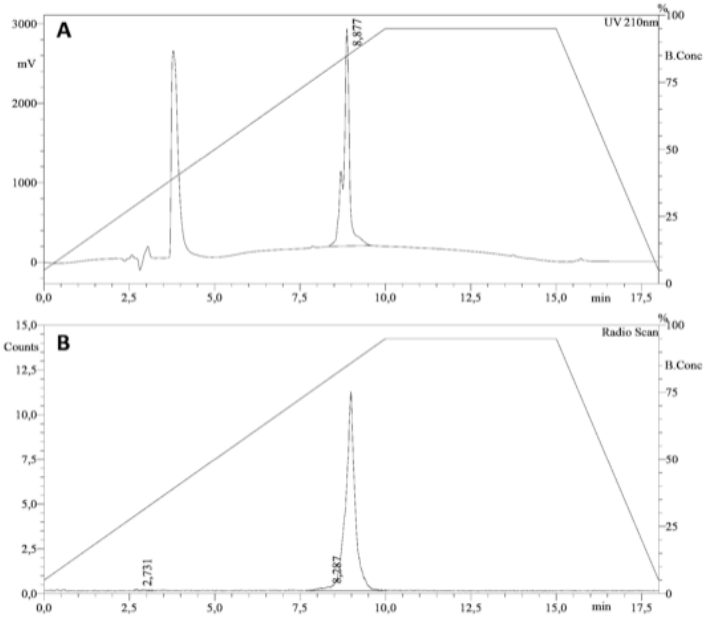

Figure 2. *HPLC chromatogram of ^{99m}Tc-HYNIC-PMB. A: UV chromatogram; B: radioactive chromatogram.*

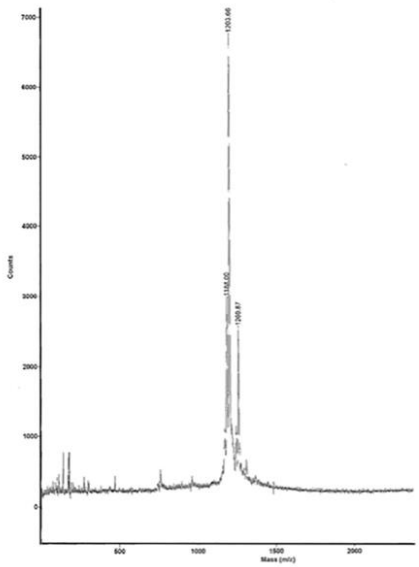

Figure 3. *Mass spectrometry analysis of conjugation HYNIC-PMB. The graph shows one peak corresponding to unconjugated PMB at 1203.6 m/z and one peak of HYNIC-conjugated PMB at 1260.8 m/z.*

The molar activity is equal to 29.5±0.6 MBq/nmole (21.7±0.4 MBq/μg). Radiolabelled PMB was stable up to 6 h both in human serum and in a 0.9% NaCl solution at 37 °C (Table 1).

Table 1. Stability of ^{99m}Tc-HYNIC-PMB in NaCl and human serum.

0.9% NaCl			Human serum		
1 h	3 h	6 h	1 h	3 h	6 h
99±1.3%	99±1.5%	98±1.8%	97±1.6%	96±1.8%	96±2.1%

MALDI-TOF analysis showed one peak corresponding to unconjugated PMB at ratio mass-to-charge (m/z) equal to 1203.66 and just one more peak of HYNIC-conjugated PMB at 1260.87 m/z (Figure 4). This data demonstrates that only 1 molecule of HYNIC is conjugated to PMB and presumably at the same position as also confirmed by HPLC analysis showing only one peak of conjugated and radiolabelled PMB.

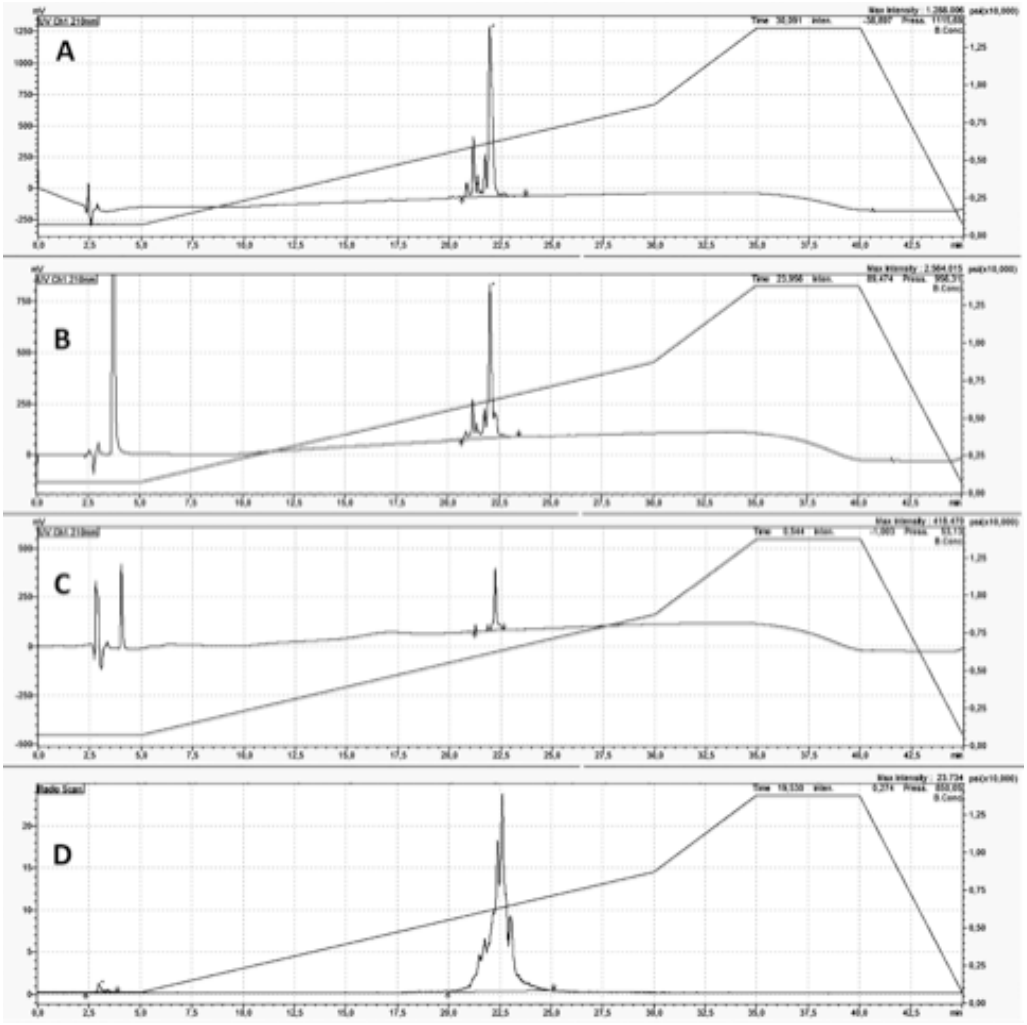

Figure 4. *HPLC analysis of different forms of PMB. Acetonitrile gradient over 45 minutes; different forms of PMB Chromatogram (UV 210 nm) of unlabelled PMB (A), chromatogram (UV 210 nm) of HYNIC-conjugated PMB (B), chromatogram (UV 210 nm) of* ^{99m}*Tc-HYNIC-PMB (C) and Radiogram (counts) of* ^{99m}*Tc-HYNIC-PMB (D). The elution profiles of unlabelled and labelled PMB were unmodified using a faster Acetonitrile gradient (21 min) as shown in Figure 2.*

3.2. In vitro binding studies

The binding test of ^{99m}Tc-HYNIC-PMB to different bacterial strains is showed in Table 2.

Table 2. *In vitro* binding of ^{99m}Tc-HYNIC-PMB in bacterial strains.

Bacterial strain	37 °C		4 °C	
	HOT	+ 100x cold	HOT	+ 100x cold
E. coli	36.2±12.5	9.9±1.7	24.2±8.6	10.4±2.7
P. aeruginosa	31.5±7.6*	12.5±5.3	32.7±11.6	17.7±9.8
A. baumanii	37.4±0.9**	5.4±8.3	28±4.3**	7.3±8.9
K. pneumoniae	45±5.7***	20.6±6.4	23.8±2.3	20.2±4.7
S. aureus	15.9±9.2	12.6±1.9	15.4±7.8	12.6±4.3
E. faecalis	18.5±8.3	19.5±4	14.8±7.9	13±1.3

Data are % CPM/CPM$_0$ (mean±SD) after 1 h incubation of ^{99m}*Tc-HYNIC-PMB with the different bacterial strains. HOT = when only radiopharmaceutical was added to bacteria; 100x cold = when 100-fold molar excess of unlabelled PMB was added to bacteria together with tracer amount of radiopharmaceutical. t test (HOT vs 100x cold) for each experimental group (37 °C, 4 °C) = *p<0.029; **p<0.01; ***p<0.005.*

Regarding the binding to P. aeruginosa, S. aureus and E. faecalis, results show that the temperature does not influence the binding. Instead, the binding to E. coli is influenced by temperature, as well as slightly for A. baumanii and K. pneumoniae. Specific displaceable binding was observed in Gram- bacteria at 37 °C and 4 °C (between 56% and 86% displaceable). In Gram+ bacteria, binding was generally lower and poorly displaceable (between 12% and 47%).

3.3. Biodistribution studies

Biodistribution studies exhibit high uptake by the kidneys, and lower signal from liver and spleen (Tables 3A and 3B).

Table 3. A) %ID/organ (mean±SD) and **B)** %ID/g (mean±SD) in tissues after ^{99m}Tc-HYNIC-PMB injection.

A) Organ	**1 h**	**3 h**	**6 h**
Blood	3.34±0.51	1.87±0.19	1.57±0.18
Small Bowel	2.88±0.21	2.01±0.36	1.20±0.01
Large Bowel	1.22±0.22	1.62±0.81	2.09±0.41
Kidneys	163.92±11.63	163.96±31.41	154.42±38.78
Spleen	11.95±2.27	8.52±8.28	12.95±4.26
Stomach	1.87±0.15	1.05±0.30	0.65±0.28
Liver	14.50±0.64	10.89±4.84	12.67±0.71
Muscle	1.48±0.45	0.63±0.13	0.67±0.07
Bone	3.02±0.30	1.55±0.41	1.38±0.32
Lungs	5.16±0.57	3.35±0.73	3.46±1.05
Salivary Glands	2.27±0.31	1.43±0.27	1.19±0.11

B) Organ	**1 h**	**3 h**	**6 h**
Blood	3.87±0.55	2.18±0.20	1.87±0.17
Small Bowel	2.34±0.19	1.67±0.45	1.21±0.03
Large Bowel	0.66±0.07	0.96±0.45	1.05±0.23
Kidneys	32.5±1.78	32.06±6.97	30.39±5.82
Spleen	0.64±0.12	0.41±0.41	0.57±0.10
Stomach	0.50±0.10	0.41±0.16	0.39±0.03
Liver	11±0.73	8.22±2.92	8.54±1.35
Muscle	0.45±0.05	0.24±0.11	0.22±0.07
Bone	0.21±0.01	0.12±0.04	0.13±0.06
Lungs	0.67±0.05	0.38±0.09	0.39±0.15
Salivary Glands	0.27±0.08	0.14±0.01	0.12±0.01

Single organ counting showed an accumulation at renal level and a large bowel activity increasing over time.

Figure 5 shows the increase of activity over time in the bladder, indicating that renal excretion also occurs.

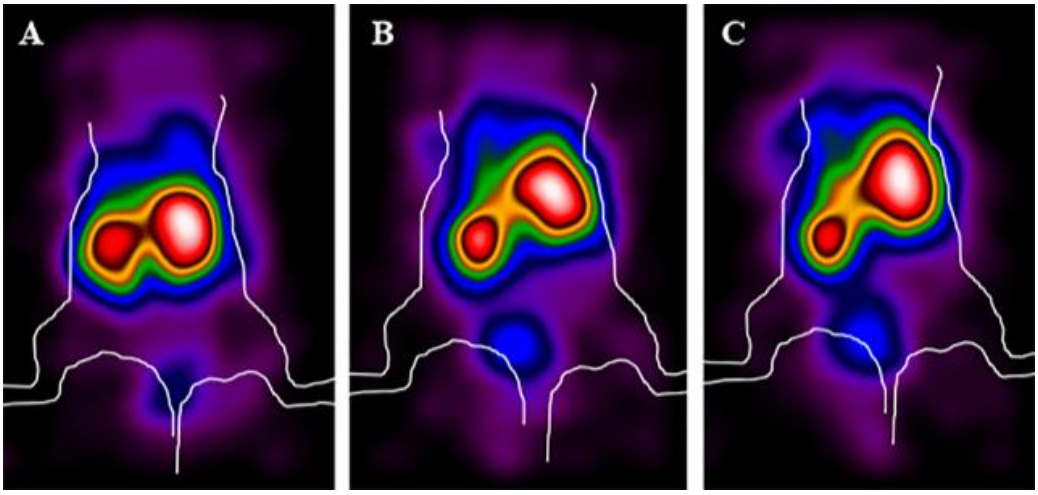

Figure 5. Representative planar γ-camera images of whole-body of healthy mice. 1 h (A), 3 h (B) and 6 h (C) p.i. of ^{99m}Tc-HYNIC-PMB showing uptake mainly in liver and kidneys with minimal excretion in the urine (bladder) over time.

3.4. Targeting studies

Figure 6 shows a representative image of uptake in the infectious focus in comparison to contralateral by zooming on lower body part of mice, acquired by high resolution planar γ-camera. In particular, S. aureus (Figure 6A) and P. aeruginosa (Figure 6B) have been chosen as representative images of uptake at 6 h p.i. and using 10^9 CFU. It is possible to appreciate how ^{99m}Tc-HYNIC-PMB accumulates in P. aeruginosa lesion (right thigh) than in contralateral left thigh or in S. aureus infected mouse.

From these images, T/B ratios were measured from the image pixel matrix for each mouse of each experiment and showed a slight increase over time for Gram- bacteria (E. coli, P. aeruginosa, A. baumanii), whereas a flat trend for Gram+ bacteria (S. aureus, E. faecalis).

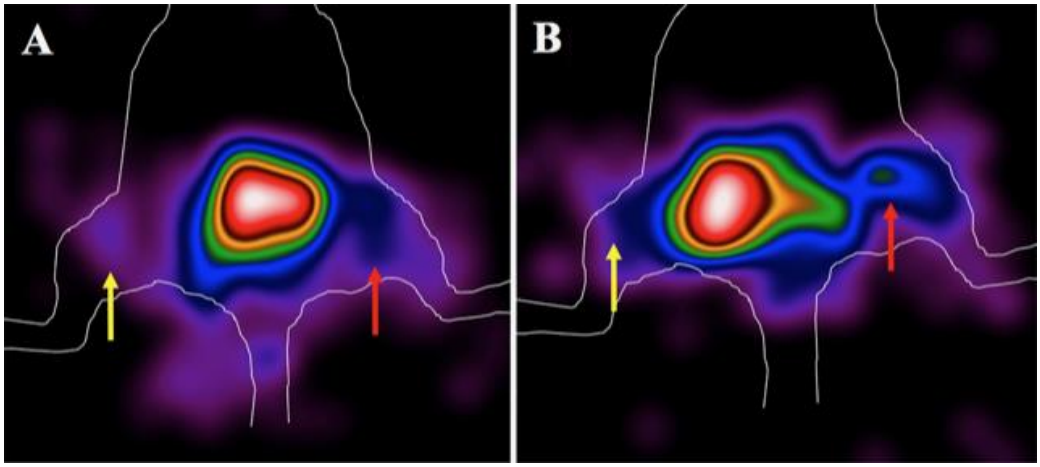

Figure 6. Representative planar γ-camera images of zoom of lower body part of two mice infected with 10^9 CFU of S. aureus (A, red arrows) and P. aeruginosa (B, red arrows) versus contralateral with only (ECM)-based hydrogel (yellow arrows) at 6 h p.i. of ^{99m}Tc-HYNIC-PMB.

At all time points, using different CFU of Gram- bacteria, it can be seen an increase of T/B ratios in relation to CFU. Conversely, for Gram+ bacteria, the increasing trend was not observed in relation to the increasing number of bacteria (Figure 7).

Indeed, there are statistically significant differences between T/B ratios of Gram- strains when compared to Gram+, especially at 6 h p.i. as reported in Table 4.

Table 4. Comparison of T/B ratios in-vivo in mice with Gram- or Gram+ infections post injection of ^{99m}Tc-HYNIC-PMB.

	1 h					
Bacterial strain	*E. faecalis*	*S. aureus*	*E. faecalis*	*S. aureus*	*E. faecalis*	*S. aureus*
	10^7		**10^8**		**10^9**	
A. baumanii	ns	ns	ns	ns	ns	ns
P. aeruginosa	ns	ns	<0.0001	0.04	ns	ns
E. coli	ns	ns	0.0008	ns	ns	ns
			3 h			
Bacterial strain	*E. faecalis*	*S. aureus*	*E. faecalis*	*S. aureus*	*E. faecalis*	*S. aureus*
	10^7		**10^8**		**10^9**	
A. baumanii	ns	ns	ns	ns	ns	ns
P. aeruginosa	ns	ns	0.0002	0.0007	0.02	0.006
E. coli	ns	ns	ns	ns	ns	ns
			6 h			
Bacterial strain	*E. faecalis*	*S. aureus*	*E. faecalis*	*S. aureus*	*E. faecalis*	*S. aureus*
	10^7		**10^8**		**10^9**	
A. baumanii	ns	ns	0.007	0.007	0.01	0.04
P. aeruginosa	ns	ns	0.01	0.027	0.001	0.001
E. coli	ns	ns	0.004	0.004	0.002	0.003

Multiple comparison was performed between different T/B from figure 4. Gram-negative (A. baumanii, P. aeruginosa, E. coli) vs Gram-positive (E. faecalis, S. aureus).

Results of ex-vivo counting of infected and contralateral thighs did not show the same results as obtained in vivo (data not shown) because of difficulty in identifying the infected area to remove. For this reason, these data were considered non-reliable and only in vivo calculated T/B are shown in Figure 7.

4. Discussion

In the last decade, a high number of studies were published about new radiopharmaceuticals able to localize infective foci by direct interaction with bacterial cells, including antimicrobial peptides, antibiotics, phages, immunoglobulins or sugars, but none of these showed high specificity or sensibility.

Many radiolabelled antibiotics have been proposed in humans, but none could be really considered "infection-specific" because of low specificity, low selectivity for a precise bacterial strain and lack of specific binding to bacteria [27]. Antimicrobial peptides, mostly UBI (29-41), have been intensively studied for bacterial infection imaging, firstly radiolabelling it with ^{99m}Tc for SPECT and, then, with ^{68}Ga for positron emission tomography (PET). Nevertheless, no conclusive results have been produced due to differences in infection models, bacterial strains, imaging protocol in preclinical and clinical studies [28-37].

All these approaches aimed at finding a new, easy to use, radiopharmaceutical for imaging infections (both due to Gram+ and Gram-) as an alternative to well-established scintigraphy with radiolabelled white blood cells (WBC) that involves patient's blood separation and several acquisitions over time. Nevertheless, the diagnostic accuracy of labelled WBC is between 90 and 98% for differential diagnosis between infection and sterile inflammation and there is no such a need of developing a new radiopharmaceutical for infection imaging [8].

Our approach has been different. We did not aim at developing an alternative to labelled WBC, but we aimed to obtain a second-line test to discriminate between Gram- and Gram+

infections to provide substantial help to clinicians for starting an appropriate antibiotic therapy, in case isolation of pathogen cannot be reached. At the moment, the same strategy has been followed by Weinstein and colleagues that used ^{18}F-fluorodeoxysorbitol ([^{18}F]FDS) to selectively image Gram- bacteria [38]. However, due to the different isotope and different animal model used we cannot compare our results with those obtained by Weinstein et al.

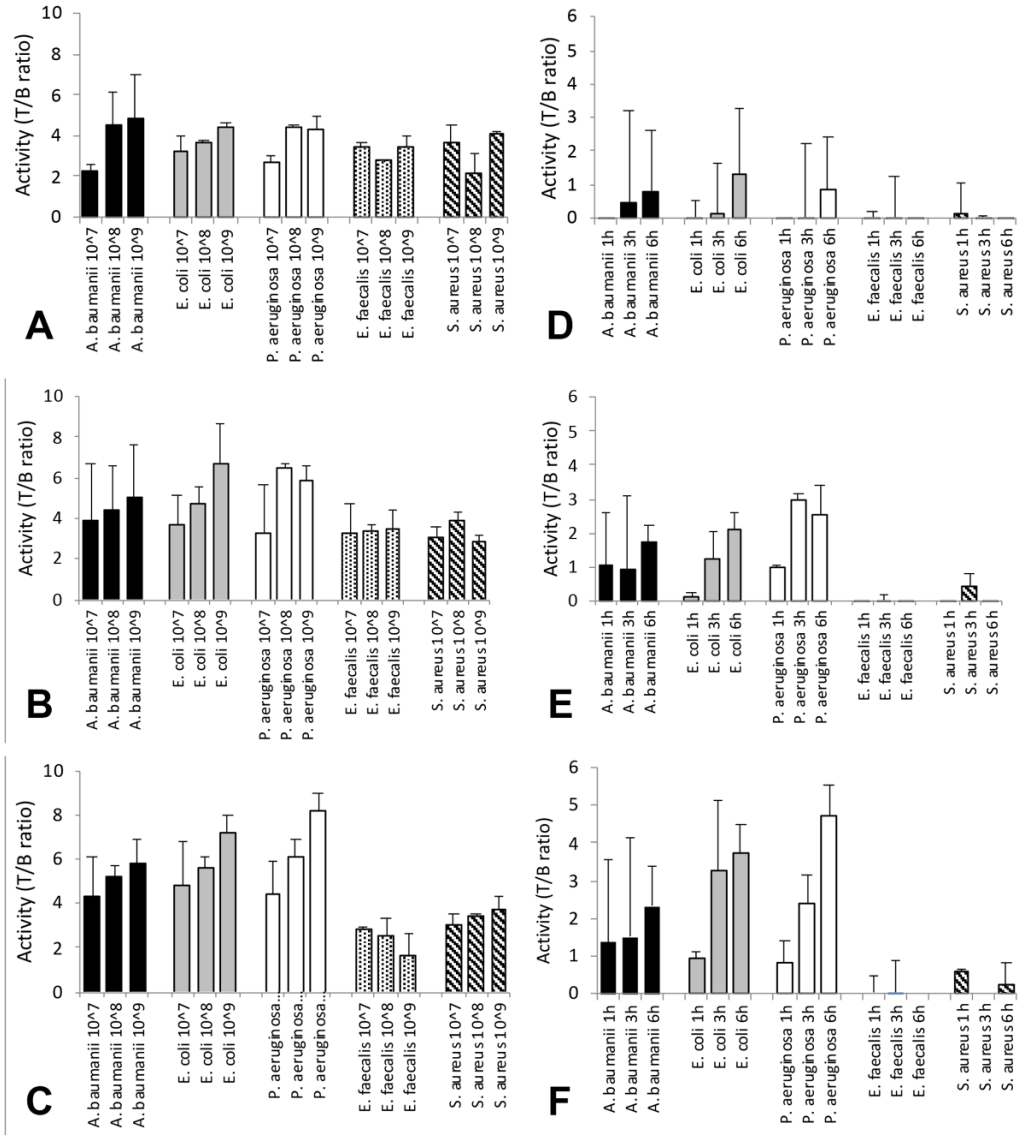

Figure 7. In vivo T/B ratios of ^{99m}Tc-HYNIC-PMB at different time points with different amounts of bacteria. A, B, C: 1 h (A), 3 h (B) and 6 h (C) p.i. A. baumanii (black), E. coli (grey), P. aeruginosa (white), E. faecalis (black dots), S. aureus (black stripes). Values are mean±SD; multiple comparison between Gram-negative (A. baumanii, E. coli, P. aeruginosa) vs Gram-positive (E. faecalis, S. aureus) was performed and reported in Table 4. C, D, E: 10^7 (C), 10^8 (D) and 10^9 (E). A. baumanii (black), E. coli (grey), P. aeruginosa (white), E. faecalis (black dots), S. aureus (black stripes). Values are mean±SD after subtraction of background activity (3.5). It can be seen that only 10^8 and 10^9 Gram- bacteria can be seen at 1, 3 and 6 h p.i. (C and D). By contrast, 10^7 bacteria (D) can be detected only at 6 h p.i.

After extensive search and several attempts, we selected PMB [39] to develop a new radiopharmaceutical for the non-invasive diagnosis of selective Gram-negative infection by gamma camera imaging. Herein, PMB has been conjugated with HYNIC as bifunctional

crosslinker and radiolabelled with ^{99m}Tc, by using tricine as co-ligand, although others (e.g. EDDA) had also been considered at an early stage. These radiolabelling conditions led to a radiopharmaceutical with high specific activity, labelling efficiency, stability and specificity for Gram- bacteria, as demonstrated by in vitro binding studies in several bacterial strains (*P. aeruginosa*, *A. baumanii* and *K. pneumonia* as Gram- and *S. aureus* and *E. faecalis* as Gram+).

The interaction between antimicrobial peptides, as PMB, and microbial plasmatic membrane is initially driven by electrostatic bounds between anionic and cationic charges, on lipid bacterial leaflet and peptide respectively [40]. Then, the amphipathic action of antimicrobial peptide induces hydrophobic interactions with consequent formation of pores that lead to internalization of antimicrobial peptide followed by binding to intracellular molecules like LPS of dead bacteria.

Based on in vitro results, we performed in vivo biodistribution studies in healthy mice that showed multiple excretion routes as also suggested by another study [41]. Indeed, ^{99m}Tc-HYNIC-PMB metabolism could be mainly hepatic (as suggested by the increasing faecal activity in the large bowel, over time), whereas the apparently stable renal activity over time could be due to a non-specific renal uptake mechanism, although some renal excretion can also occur (as suggested by the increasing bladder activity, over time). This activity in the bladder does not correspond to an increase of activity in the stomach and salivary glands that, on the contrary, is considerably reduced over time (Table 3B). These findings suggest that some renal excretion of ^{99m}Tc-HYNIC-PMB, or of a ^{99m}Tc-labelled degradation product, occurs.

Furthermore, we performed in vivo targeting studies, inducing infection with same Gram- and Gram+ bacterial strains, injected with (ECM)-based hydrogel in the right thigh of the mouse. These experiments showed significantly higher uptake in the infectious site when using Gram- bacteria than Gram+ ones, both in relation to the increased number of bacteria and over time, as showed by T/B ratios in Figure 6. In particular, the best time point for imaging mice was 6 h p.i. and the best number of CFU detected was 10^8 to 10^9. Nevertheless, also Gram+ bacteria showed a non-specific uptake, that should be taken into consideration in case of human studies as potential factor that may reduce the sensitivity of imaging. If non-specific binding is subtracted from data in Figure 4, it appears more evident that 10^8 and 10^9 Gram- bacteria can be visualized both at 1, 3 and 6 h p.i. but 10^7 bacteria can only be detected at 6 h p.i. (Figure 7D, 7E and 7F). In these graphs, the background threshold is randomly selected but mostly important the graphs show that a Gram- infection can be distinguished from a Gram+ infection by considering an uptake over a certain threshold. The level of the threshold will probably depend on the type of infection, the site and animal model used.

The reason why ex-vivo results of infected and contralateral thighs did not confirm the results obtained in vivo, could stand on the fact that inflamed tissues to be removed from infected thighs were very difficult to identify and of variable size and weight. This can be due to a different degree of leukocytic infiltration and oedema or generally to a host response to injury. Inflamed areas were generally larger in thighs infected with 10^9 bacteria and in thighs infected with *A. baumanii* and smaller in Gram+ infected thighs. This variability in resected tissues resulted in a high variability of weights, and, as a consequence, a high variability of %ID/g and T/B ratios. For this reason, these data were considered non-reliable in contrast to in vivo measurement of thigh activity by drawing the same ROI over the infected and non-infected thighs.

Best images were obtained using 10^8 CFU of *P. aeruginosa*, at 3 and 6 h p.i., whereas, for *A. baumanii* and *E. coli*, higher number of bacteria and late imaging time point (6 h p.i.) was needed to reach comparable results. Therefore, a detectability limit could exist for which bacterial amount lower than 10^8 CFU are more difficult to detect. We should also consider

that in humans, bacteria are spread (as in infected prosthesis and osteomyelitis) and not always localized (as in case of endocarditis) and may also produce biofilm that may further reduce the sensitivity of the technique.

Therefore, a radiopharmaceutical with high specific activity is necessary in order to inject a reasonable amount of radioactivity avoiding pharmacological side effects.

A possible criticism to the present study could be that the animal model we used does not well represent a human infection. However, we chose this model as an initial easy screening model for the evaluation of the specificity of ^{99m}Tc-HYNIC-PMB. In future, we will study model of osteomyelitis [42] or model with infected subcutaneous Teflon cage, as previously described [28] and according to recently published suggestions [43].

In addition, following the experience of ^{68}Ga-radiolabelled antimicrobial peptides [5, 44-46] and considering the fast binding of PMB to bacteria and fast metabolic clearance, we may consider labelling PMB with ^{68}Ga for PET applications.

5. Conclusions

In the present study, we radiolabelled PMB with high specific activity, efficiency and stability. In vitro, the radiopharmaceutical showed a good specificity for Gram- bacteria in comparison to Gram+ ones as negative controls. In vivo, ^{99m}Tc-HYNIC-PMB was excreted through multiple metabolic routes. Targeting studies confirmed the results obtained in vitro showing statistically significant differences between Gram- and Gram+ infected mice, suggesting ^{99m}Tc-HYNIC-PMB as potential agent for identification of Gram- infections. Further investigations are needed to investigate the in vivo sensitivity and specificity of ^{99m}Tc-HYNIC-PMB in other animal models and in humans**.**

Author Contributions: Conceptualization, A.S., S.A. and I.S.; Methodology, S.A., F.G., M.V., M.C. and D.M.; Statistical analysis, G.C.; Writing first draft, S.A. and F.G.; Writing – Review & Editing Supervision, A.S. All authors read and approved the final manuscript.

Funding: This study was funded by "Sapienza" University of Rome.

Data Availability Statement: All data are available from our statistician G.C.

Acknowledgments: Authors wish to acknowledge the Animal Facility of University Tor Vergata of Rome for providing support during animal studies and "Sapienza" University of Rome for providing financial support for this study.

Conflicts of Interest: The authors declare no conflict of interest.

References

1. Auletta, S.; Varani, M.; Horvat, R.; Galli, F.; Signore, A.; Hess, S. PET radiopharmaceuticals for specific bacteria imaging: a systematic review. *J Clin Med* **2019**, *8*, 197.
2. Zhang, H.; Jiang, N.; Zhu, L. Experimental studies on imaging of infected site with ^{99m}Tc-labeled ciprofloxacin in mice. *Chin Med J* **2009**, *122*, 1907-1909.
3. Langer, O.; Brunner, M.; Zeitlinger, M.; Ziegler, S.; Muller, U.; Dobrozemsky, G.; Lackner, E.; Joukhadar, C.; Mitterhauser, M.; Wadsak, W.; Minar, E.; Dudczak, R.; Kletter, K.; Muller, M. In vitro and in vivo evaluation of [^{18}F]ciprofloxacin for the imaging of bacterial infections with PET. *Eur J Nucl Med Mol Imaging* **2005**, *32*, 143-150.
4. Li, J, Zheng, H.; Fodah, R.; Warawa, J.M.; Ng, C.K. Validation of 2-^{18}F-Fluorodeoxysorbitol as a potential radiopharmaceutical for imaging bacterial infection in the lung. *J Nucl Med* **2018**, *59*, 134-139.
5. Vilche, M.; Reyes, A.L.; Vasilskid, E.; Oliver, P.; Balter, H.; Engler, H. ^{68}Ga-NOTA-UBI-29-41 as a PET tracer for detection of bacterial infection. *J Nucl Med* **2016,** *57*, 622-627.
6. de Vries, E.F.J.; Roca, M.; Jamar, F.; Israel, O.; Signore, A. Guidelines for the labelling of leukocytes with ^{99m}Tc-HMPAO. *Eur J Nucl Med Mol Imaging* **2010**, *37*, 842-848.
7. Roca, M.; de Vries, E.F.J.; Jamar, F.; Israel, O.; Signore, A. Guidelines for the labelling of leukocytes with ^{111}In-oxine. *Eur J Nucl Med Mol Imaging* **2010**, *37*, 835-841.
8. Glaudemans, A.W.; Prandini, N.; di Girolamo, M.; Argento, G.; Lauri, C.; Lazzeri, E.; Muto, M.; Sconfienza, L.M.; Signore, A. Hybrid imaging of musculoskeletal infections. *Q J Nucl Med Mol Imaging* **2018**, *62*, 3-13.
9. Eisler, T.; Svensson, O.; Engström, C.F.; Reinholt, F.P.; Lundberg, C.; Wejkner, B.; Schmalholz, A.; Elmstedt, E. Ultrasound for diagnosis of infection in revision total hip arthroplasty. *J Arthroplast* **2001**, *16*, 1010-1017.
10. Battaglia, M.; Vannini, F.; Guaraldi, F.; Rossi, G.; Biondi, F.; Sudanese, A. Validity of preoperative ultrasound-guided aspiration in the revision of hip prosthesis. *Ultrasound Med Biol* **2011**, *37*, 1977-1983.

11. Tomas, X.; Bori, G.; Garcia, S.; Garcia-Diez, A.I.; Pomes, J.; Soriano, A.; Ríos, J.; Almela, M.; Mensa, J.; Gallart, X.; Martinez, J.C.; Riba, J. Accuracy of CT-guided joint aspiration in patients with suspected infection status post-total hip arthroplasty. *Skeletal Radiol* **2011**, *40*, 57-64.
12. Meermans, G.; Haddad, F.S. Is there a role for tissue biopsy in the diagnosis of periprosthetic infection? *Clin Orthop Relat Res* **2010**, *468*, 1410-1417.
13. Jordan, R.W.; Smith, N.A.; Saithna, A.; Sprowson, A.P.; Foguet, P. Sensitivities, specificities and predictive values of microbiological culture techniques for the diagnosis of prosthetic joint infection. *BioMed Res Int* **2014**, *2014*, 180416.
14. Ainsworth, G.C.; Brown, A.M.; Brownlee, G. Aerosporin, an antibiotic produced by Bacillus aerosporus Greer. *Nature* **1947**, *160*, 263.
15. Stansly, P.G.; Shepherd, R.G.; White, H.J. Polymyxin: a new chemotherapeutic Agent. Bull. *Johns Hopkins Hosp* **1947**, *81*, 43-54.
16. Benedict, R.G; Langlykke, A.F. Antibiotic activity of Bacillus polymyxa. *J Bacteriol* **1947**, *54*, 24-25.
17. Newton, B.A. The properties and mode of action of the polymyxins. *Bacteriol Rev* **1956**, *20*, 14-27.
18. Falagas, M.E.; Kasiakou, S.K. Toxicity of polymyxins: a systematic review of the evidence from old and recent studies. C*rit Care* **2006**, *10*, R27.
19. Velkov, T.; Thompson, P.E.; Nation, R.L.; Li, J. Structure-activity relationships of polymyxin antibiotics. *J Med Chem* **2010**, *53*, 1898-916.
20. Falagas, M.E.; Rafailidis, P.I.; Matthaou, D.K. Resistance to polymyxins: Mechanisms, frequency and treatment options. *Drug Resistance Updates* **2010**, *13*, 132-138.
21. Orwa, J.A.; Govaerts, C.; Busson, R.; Roets, E.; Van Schepdael, A.; Hoogmartens, J. Isolation and structural characterization of polymyxin B components. *J Chromatogr A* **2001**, *912*, 369-373.
22. Kwa, A.; Tam, V.H.; Falagas, M.E. Polymyxins: a review of the current status including recent developments. *Annals Academy of Medicine Singapore* **2008**, *37*, 870-883.
23. Li, J.; Nation, R.L., Turnidge, J.D.; Milne, R.W.; Coulthard, K.; Rayner, C.R.; Paterson, D.L. Colistin: the reemerging antibiotic for multidrug-resistant Gram-negative bacterial infections. *Lancet Infect Dis* **2006**, 6, 589-601.
24. Zavascki, A.P.; Goldani, L.Z.; Li, J.; Nation, R.L. Polymyxin B for the treatment of multidrug-resistant pathogens: a critical review. *J Antimicrob Chemother* **2007**, 60, 1206-1215.
25. Rennen, H.J.; Boerman, O.C.; Koenders, E.B.; Oyen, W.J.; Corstens, F.H. Labeling proteins with Tc-99m via hydrazinonicotinamide (HYNIC): optimization of the conjugation reaction. *Nucl Med Biol* **2000**, 27, 599-604.
26. Cao, J.; Zhao, L.; Li, Y.; Liu, Y.; Xiao, W.; Song, Y.; Luo, L.; Huang, D.; Yancopoulos, J.D.; Wiegand, S.J.; Wen, R. A subretinal Matrigel rat choroidal neovascularization (CNV) model and inhibition of CNV and associated inflammation and fibrosis by VEGF trap. *Invest Ophthalmol Vis Sci* **2010**, 51, 6009-6017.
27. Auletta, S.; Galli, F.; Lauri, C.; Martinelli, D.; Santino, I.; Signore, A. Imaging bacteria with radiolabelled quinolones, cephalosporins and siderophores for imaging infection: a systematic review. *Clin Transl Imaging* **2016**, 4, 229-252.
28. Auletta, S.; Baldoni, D.; Varani, M.; Galli, F.; Hajar, I.A.; Duatti, A.; Ferro-Flores, G.; Trampuz, A.; Signore, A. Comparison of ^{99m}Tc-UBI 29-41, ^{99m}Tc-ciprofloxacin, ^{99m}Tc-ciprofloxacin dithiocarbamate and ^{111}In-biotin for targeting experimental Staphylococcus aureus and Escherichia coli foreign-body infections: an ex-vivo study. *Q J Nucl Med Mol Imaging* **2019**, *63*, 37-47.
29. Ferro-Flores, G.; Arteaga de Murphy, C.; Pedraza-López, M.; Meléndez-Alafort, L.; Zhang, Y.M.; Rusckowski, M; Hnatowich, D.J. In vitro and in vivo assessment of ^{99m}Tc-UBI specificity for bacteria. *Nucl Med Biol* **2003**, *30*, 597-603.
30. Meléndez-Alafort L.; Nadali A.; Pasut G.; Zangoni E.; De Caro R.; Cariolato L.; Giron, M.C.; Castagliuolo, I.; Veronese, F.M.; Mazzi, U. Detection of sites of infection in mice using ^{99m}Tc-labeled PN(2)S-PEG conjugated to UBI and ^{99m}Tc-UBI: a comparative biodistribution study. *Nucl Med Biol* **2009**, *36*, 57-64.
31. Welling, M.M.; Mongera, S.; Lupetti, A.; Balter, H.S.; Bonetto, V.; Mazzi, U.; Pauwels, E.K.; Nibbering, P.H. Radiochemical and biological characteristics of ^{99m}Tc-UBI 29-41 for imaging of bacterial infections. *Nucl Med Biol* **2002**, *29*, 413-422.
32. Akhtar, M.S.; Iqbal, J.; Khan, M.A.; Irfanullah, J.; Jehangir, M.; Khan, B.; Ul-Haq, I.; Muhammad, G.; Nadeem, M.A.; Afzal, M.S.; Imran, M.B. ^{99m}Tc-labeled antimicrobial peptide ubiquicidin (29-41) accumulates less in Escherichia coli infection than in Staphlococcus aureus infection. *J Nucl Med* **2004**, *45*, 849-856.
33. Sarda-Mantel, L.; Saleh-Mghir, A.; Welling, M.M.; Meulemans, A.; Vrigneaud, J.M.; Raguin, O.; Hervatin, F.; Martet, G.; Chau, F.; Lebtahi, R.; Le Guludec, D. Evaluation of ^{99m}Tc-UBI 29-41 scintigraphy for specific detection of experimental Staphylococcus aureus prosthetic joint infections. *Eur J Nucl Med Mol Imaging* **2007**, *34*, 1302-1309.
34. Akhtar, M.S.; Qaisar, A.; Irfanullah, J.; Iqbal, J.; Khan, B.; Jehangir, M.; Nadeem, M.A.; Khan, M.A.; Afzal, M.S.; Ul-Haq, I.; Imran, M.B. Antimicrobial peptide ^{99m}Tc-ubiquicidin 29-41 as human infection imaging agent: clinical trial. *J Nucl Med* **2005**, *46*, 567-573.
35. Meléndez-Alafort, L.; Rodríguez-Cortés, J.; Ferro-Flores, G.; Arteaga De Murphy, C.; Herrera-Rodríguez, R.; Mitsoura, E.; Duncker, C.M. Biokinetics of (99m)Tc-UBI 29-41 in humans. *Nucl Med Biol* **2004**, *31*, 373-379.
36. Gandomkar, M.; Najafi, R.; Shafiei, M.; Mazidi, M.; Goudarzi, M.; Mirfallah, S.H.; Ebrahimi, F.; Heydarpor, H.R.; Abdie, N. Clinical evaluation of antimicrobial peptide [(99m)Tc/Tricine/HYNIC(0)]ubiquicidin 29-41 as a human-specific infection imaging agent. *Nucl Med Biol* **2009**, *36*, 199-205.
37. Sathekge, M.; Garcia-Perez, O.; Paez, D.; El-Haj, N.; Kain-Godoy, T.; Lawal, I., Estrada-Lobato, E. Molecular imaging in musculoskeletal infections with ^{99m}Tc-UBI 29-41 SPECT/CT. *Ann Nucl Med* **2018**, *32*, 54-59.

38. Weinstein, E.A.; Ordonez, A.A.; De Marco, V.P.; Murawski, A.M.; Pokkali, S.; MacDonald, E.M.; Klunk, M.; Mease, R.C.; Pomper, M.G.; Jain, S.K. Imaging Enterobacteriaceae infection in vivo with 18F-fluorodeoxysorbitol positron emission tomography. *Sci Transl Med* **2014**, *6*, 259ra146.
39. Vaara, M. New polymyxin derivatives that display improved efficacy in animal infection models as compared to polymyxin B and colistin. *Med Res Rev* **2018**, *38*, 1661-1673.
40. Yeaman, M.R.; Yount, N.Y. Mechanisms of antimicrobial peptide action and resistance. *Pharmacol Rev* **2003**, *55*, 27-55.
41. Abdelraouf, K.; He, J.; Ledesma, K.R.; Hu, M.; Tam, V.H. Pharmacokinetics and renal disposition of polymyxin B in an animal model. *Antimicrob Agents Chemother* **2012**, *56*, 5724-5727.
42. Thompson, J.M.; Thorek, D.L.J.; Miller, L.S. Mouse model of Gram-negative prosthetic joint infection reveals therapeutic targets. *JCI Insight* **2018**, *3*, e121737.
43. Signore, A.; Artiko, V.; Conserva, M.; Ferro-Flores, G.; Welling, M.M.; Jain, S.K.; Hess, S.; Sathekge, M. Imaging bacteria with radiolabelled probes: is it feasible? *J Clin Med* **2020**, *9*, 2372.
44. Mukherjee, A.; Bhatt, H.; Shinto, A.; Korde, A.; Kumar, M.; Kamaleshwaran, K.; Joseph, J.; Sarma, H.D.; Dash, A. ^{68}Ga-NOTA-ubiquicidin fragment for PET imaging of infection: From bench to bedside. *J Pharm Biomed Anal* **2018**, *159*, 245-251.
45. Ebenhan, T.; Sathekge, M.M.; Lwngana, T.; Koole, M.; Gheysens, O.; Govender, T.; Zeevaart, J.R. ^{68}Ga-NOTA-functionalized Ubiquicidin: cytotoxicity, biodistribution, radiation dosimetry, and first-in-human PET/CT imaging of infections. *J Nucl Med* **2018**, *59*, 334-339.
46. Bhatt, J.; Mukherjee, A.; Korde, A.; Kumar, M.; Sarma, H.D.; Dash, A. Radiolabeling and preliminary evaluation of Ga-68 labeled NODAGA-Ubiquicidin fragments for prospective infection imaging. *Mol Imaging Biol* **2017**, *19*, 59-67.